Supporting Information

Perry et al. 10.1073/pnas.0906597106

SI Methods

Voltage Clamp. Currents were recorded from oocytes 1–5 days after cRNA injection by using the two-electrode voltage-clamp technique (1). Agarose cushion microelectrodes were fabricated by filling borosilicate pipette tips with 1% agarose dissolved in 3 M KCl and then back-filling with 3 M KCl (2). Oocytes were voltage clamped to a holding potential of −110 mV, and 3-s pulses to 0 mV were applied every 15 s until current magnitude reached a steady-state level. To determine the voltage dependence of inactivation, a 2-s prepulse to +40 mV was followed by repolarization to a test potential (Vt) that was varied from +30 mV to −140 mV and applied in 10-mV increments. The peak of the tail currents were then plotted as a function of Vt to obtain the fully activated I-V relationship. Inward rectification of hERG1 was quantified by the deviation of the tail current amplitudes from the maximum slope conductance of the fully activated I-V relationship, estimated from a linear fit of peak tail current values measured at Vt between −140 and −110 mV. Deviation of the I-V relationships from linearity was corrected by the driving force for K^+ (Vt − Vrev) to obtain a rectification factor for each value of Vt (3). The plot of rectification factor versus Vt was fitted with a Boltzmann function to obtain the half-point ($V_{0.5}$) and slope factor (k) for the voltage dependence of hERG1 inactivation. Other voltage pulse protocols are described under *Results* and in the figure legends. After addition of PD-118057 to the bathing solution, 3-s pulses to 0 mV were applied every 15 s until a new steady-state level was achieved. Relevant voltage protocols were then repeated in the presence of drug.

Gating currents were measured using the cut-open oocyte Vaseline gap (COVG) method (4) as described previously (5). Signals were low-pass filtered at 10 kHz and digitized at 40 kHz. Linear leak and capacitance currents were compensated by analog circuitry and subtracted online by using a p/-8 protocol. Single hERG1 channel currents were measured in cell-attached patches, as described previously (6), using an Axopatch 200B amplifier (Molecular Devices, Sunnyvale, CA) and an electrode resistance of 8–15 MΩ when filled with pipette solution. Single channel current amplitudes were determined from analysis of all-points amplitude histograms of currents filtered at 1 kHz and digitized at 5 kHz.

Molecular Modeling. Modeling and docking were performed with the Insight II modules Homology, Builder, and Docking (version 8.2, Accelrys, San Diego, CA). The crystal structure of the mammalian Shaker Kv1.2 potassium channel subunit complex (PDB ID 2A79) and a previously published alignment for S6 and the SF (7) were used for creating a hERG1 homology model. The S5 alignment was based on assigning E575 to the C-terminal end of the domain. The PD-118057 structure was energy optimized. Interactions of the ligand with residues from two adjacent hERG1 subunits including their S4-S5 linker, S5, SF, and S6 were determined by molecular docking at a maximal distance of 15 Å from residue C643 in hERG1. The docking was initiated from random configurations (n = 200) of the ligand. Residues of the hERG1 subunits and the ligand were flexible during the optimization procedure. The consistent valence force field (CVFF) was used to calculate conformational energies. Optimal configurations were determined by using simulated annealing techniques with an initial temperature of 400°K and a final temperature of 300°K followed by final minimization (steps = 1,000).

1. Stühmer W (1992) Electrophysiological recording from *Xenopus* oocytes. *Methods Enzymol* 207:319–339.
2. Schreibmayer W, Lester HA, Dascal N (1994) Voltage clamping of *Xenopus laevis* oocytes utilizing agarose-cushion electrodes. *Pflugers Arch* 426:453–458.
3. Sanguinetti MC, Jiang C, Curran ME, Keating MT (1995) A mechanistic link between an inherited and an acquired cardiac arrhythmia: *HERG* encodes the I_{Kr} potassium channel. *Cell* 81:299–307.
4. Stefani E, Bezanilla F (1998) *Methods in Enzymology*, ed. Conn PN (Academic, San Diego), pp. 300–318.
5. Piper DR, Varghese A, Sanguinetti MC, Tristani-Firouzi M (2003) Gating currents associated with intramembrane charge displacement in HERG potassium channels. *Proc Natl Acad Sci USA* 100:10534–10539.
6. Zou A, Curran ME, Keating MT, Sanguinetti MC (1997) Single HERG delayed rectifier K^+ channels in *Xenopus* oocytes. *Am J Physiol* 272:H1309–H1314.
7. Perry M, Sachse FB, Sanguinetti MC (2007) Structural basis of action for a human ether-a-go-go-related gene 1 potassium channel activator. *Proc Natl Acad Sci USA* 104:13827–13832.

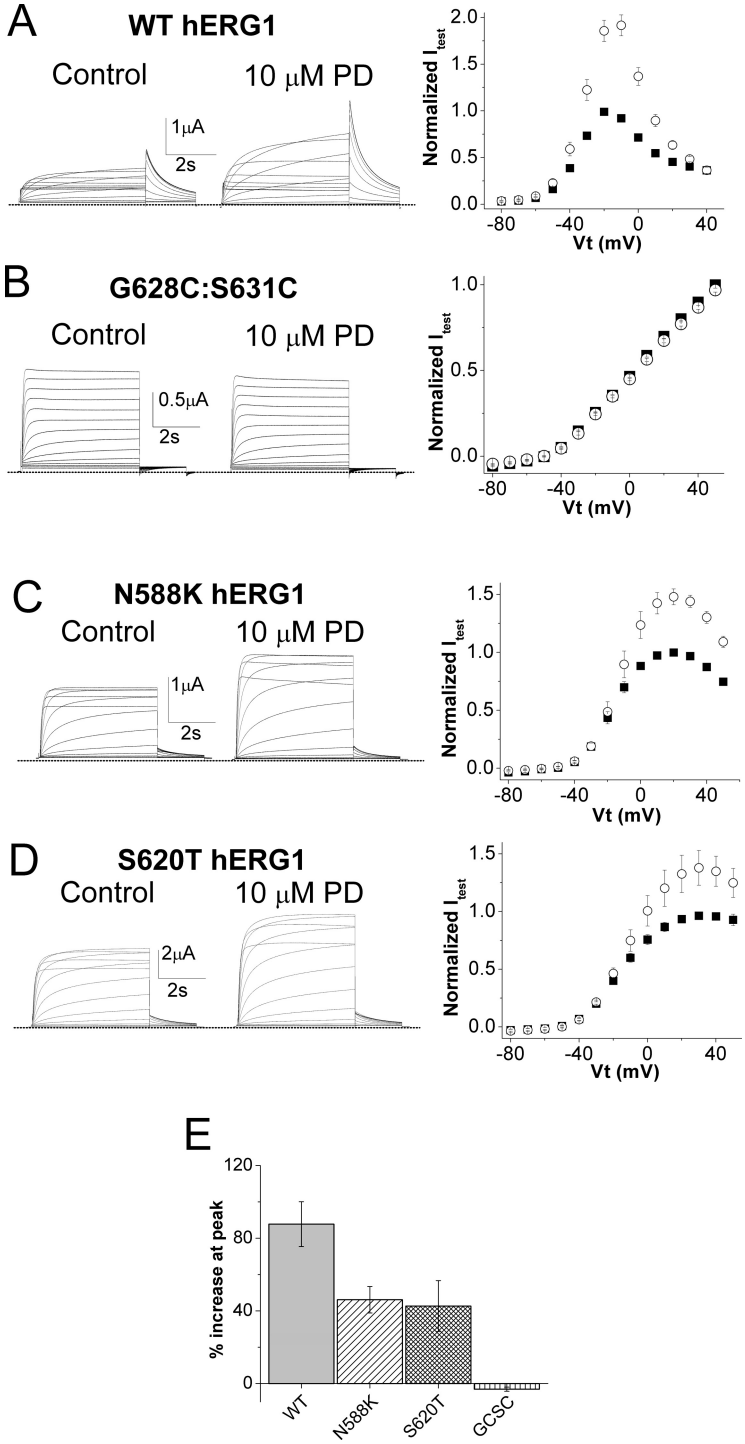

Fig. S1. Mutant channels with impaired inactivation are less sensitive to PD-118057. (*A*) PD-118057 does not activate G628C/S631C hERG1 mutant channels that do not inactivate and have altered ion selectivity. (*Left*) WT hERG1 currents recorded before (control) and after 10 μM PD-118057. (*Right*) Mean *I-V* relationships ($n = 7$) for currents at the end of the 5-s test pulse determined before (filled squares) and after 10 μM PD-118057. (*B*) (*Left*) G628C/S631C hERG1 currents recorded before (control) and after 10 μM PD-118057. (*Right*) Mean *I-V* relationships ($n = 5$) for currents at the end of the 5-s test pulse determined before (filled squares) and after 10 μM PD-118057. At a *V*t of 0 mV, mutant channel current was decreased $-3.2 \pm 2.6\%$ by the drug ($n = 5$). For both channel types, currents were elicited using pulse protocol described in legend for Fig. 1*F*, and *I-V* relationships were normalized relative to peak value of control tail currents. (*C* and *D*) Effects of PD-118057 on N588K and S620T hERG1 channels. Current traces (protocol as Fig. 1*F*) and mean *I-V* relationships for N588K (*C*, $n = 3$) and S620T (*D*, $n = 5$) hERG1 channels before (filled square) and after 10 μM PD-118057 (open square). *I-V* relationships were normalized relative to peak outward tail current in control. (*E*) Percent increase in current magnitude, determined from the peak of the *I-V* relationship for WT and inactivation impaired hERG1 channels.

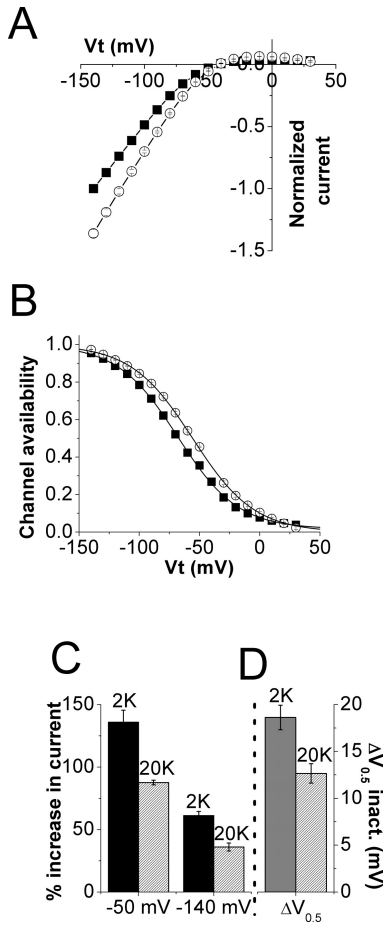

Fig. S2. Elevated $[K^+]_e$ attenuates the effects of PD-118057 on WT hERG1 channel current. (*A*, *B*) Fully activated *I-V* relationship (*A*) and corresponding voltage dependence of inactivation (*B*) recorded from oocytes bathed in a solution with elevated (20 mM) $[K^+]_e$, before (filled squares) and after 10 μM PD-118057 (open circles). (*C*) Comparison of the effect of 10 μM PD-118057 when recorded in solution with 2 mM $[K^+]_e$ (*solid bar*) or 20 mM $[K^+]_e$ (*hatched bar*). Percent increase in current magnitude at the indicated V_t (in mV) and $[K^+]_e$ (in mM). (*D*) The PD-118057 induced shift in $V_{0.5}$ for inactivation for $[K^+]_e$ = 2 or 20 mM.

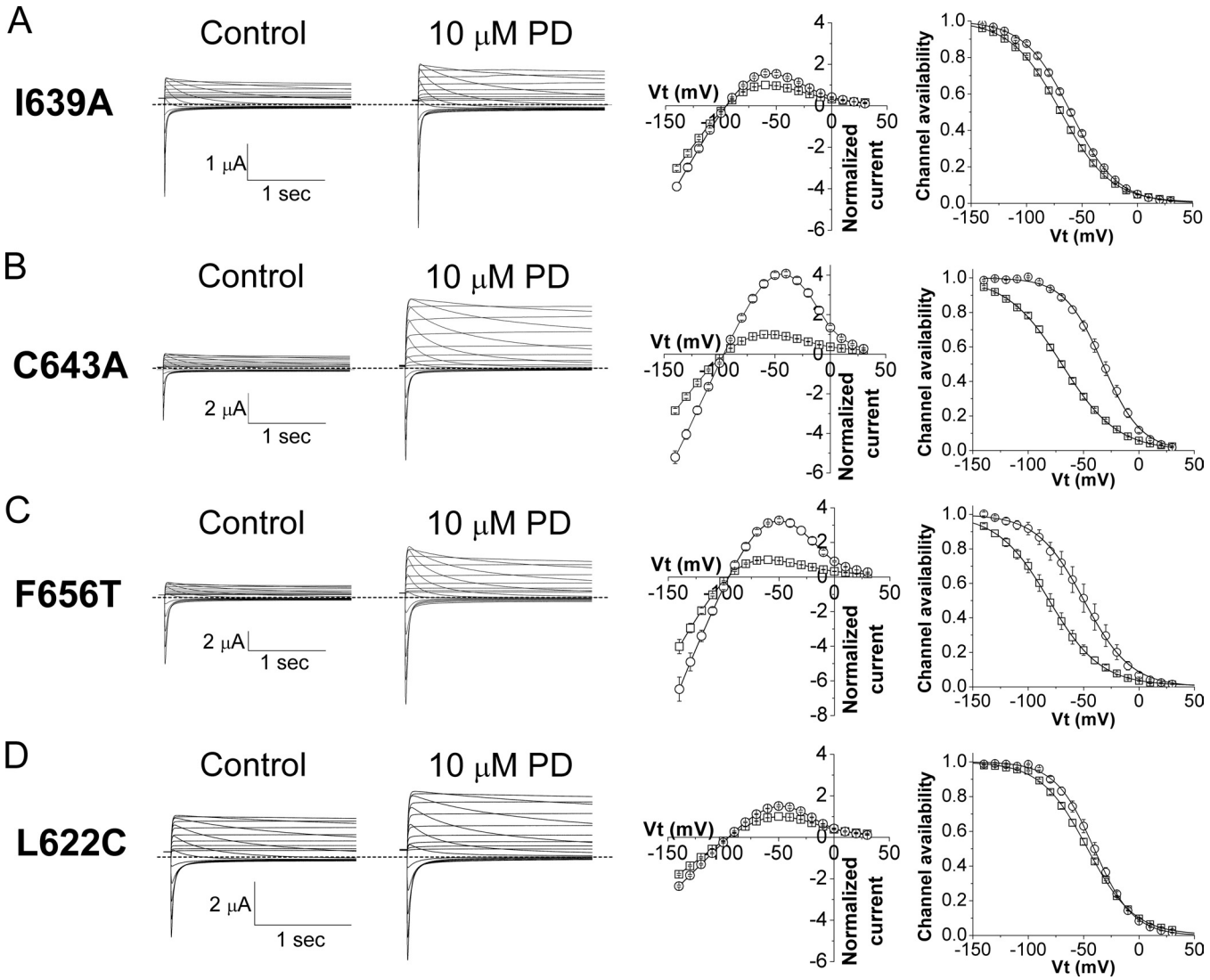

Fig. S3. Effect of PD-118057 on selected hERG1 mutant channels. (*A-D*) Current traces (elicited as described in Fig. 1*A*), mean fully activated *I-V* relationships, and corresponding voltage dependence of inactivation shown before (open squares) and after 10 μM PD-118057 (open circles) for I639A (*A*), C643A (*B*), F656T (*C*), and L622C (*D*) mutant hERG1 channels.

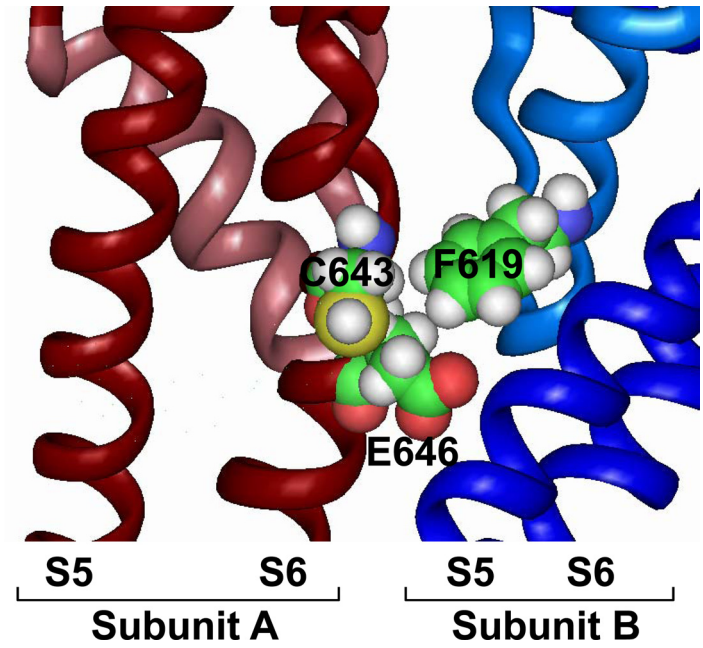

Fig. S4. Homology model of the pore module for two adjacent subunits of the L646E hERG1 mutant channel. Glu in this position occludes the binding pocket for PD-118057.

Table S1. Summary of effects of PD-118057 on the voltage dependence of inactivation for wild-type (WT) and mutant hERG1 channels

	Control		10 μM PD			
Channel type	$V_{0.5}$ inact (mV)	Slope factor (mV)	$V_{0.5}$ inact (mV)	Slope factor (mV)	$\Delta V_{0.5}$ PD (mV)	*N*
WT hERG1	−52.9 ± 1.8	20.9 ± 0.2	−34.2 ± 2.4	16.3 ± 0.3	+18.6 ± 1.4	7
DMSO Control	−48.5 ± 6.2	19.7 ± 0.3	−48.7 ± 7.0	19.2 ± 0.6	−0.1 ± 1.5	3
S5 Helix						
F557L	−70.7 ± 2.3	32.8 ± 0.3	−43.5 ± 5.3	28.8 ± 0.9	+27.2 ± 3.3	3
A558V	−23.4 ± 1.8	19.7 ± 1.5	−13.2 ± 1.3	16.8 ± 0.2	+10.2 ± 1.1	3
L559A	−54.2, −50.4	21.6, 18.5	−37.6, −31.2	17.1, 14.9	+16.6, +19.2	2
I560A	−36.1 ± 3.9	20.7 ± 1.1	−23.2 ± 1.1	17.2 ± 0.7	+12.9 ± 2.9	3
A561G	−24.8 ± 1.7	18.4 ± 0.6	−19.0 ± 2.4	15.8 ± 0.7	+5.8 ± 1.1	3
H562A, C, K	No expression					
W563A	−52.7, −63.8	20.4, 20.5	−39.4, −45.2	17.1, 17.3	+13.3, +18.5	2
L564A	−7.0, −11.0	16.0, 17.9	+3.7, −2.7	13.0, 13.3	+10.7, +8.3	2
A565G	−38.0 ± 3.6	20.1 ± 1.0	−24.6 ± 4.0	16.0 ± 0.5	+13.5 ± 0.8	4
C566A	−43.5 ± 1.9	18.6 ± 0.2	−36.3 ± 0.7	16.4 ± 0.6	+7.1 ± 1.2	3
I567A	−42.1, −38.9	22.4, 21.3	−26.3, −20.2	16.6, 14.4	+15.7, +18.7	2
W568A	No expression					
Y569A	−62.1 ± 2.6	21.6 ± 1.0	−42.0 ± 3.7	16.3 ± 1.4	+20.1 ± 2.5	3
Pore helix						
F619A	−36.5 ± 1.0	16.9 ± 0.5	−39.2 ± 0.8	18.6 ± 0.6	−2.7 ± 0.9	5
I622C	−46.9 ± 1.3	20.8 ± 0.5	−40.8 ± 2.3	17.2 ± 0.7	+6.1 ± 1.0	5
S6 Helix						
I639A	−69.1 ± 1.3	22.5 ± 0.3	−60.2 ± 1.1	20.9 ± 0.3	+8.9 ± 1.0	5
F640C	−40.6 ± 0.7	17.9 ± 0.4	−26.0 ± 1.2	14.8 ± 0.6	+14.6 ± 0.8	4
S641C	*High K					3
I642C	−37.2 ± 1.5	15.4 ± 0.3	−27.2 ± 1.3	14.2 ± 0.8	+10.0 ± 1.7	3
C643A	−69.6 ± 1.5	24.9 ± 0.2	−32.6 ± 2.6	16.9 ± 0.2	+37.0 ± 1.6	5
V644A	−12.3 ± 2.9	15.0 ± 0.2	−4.5 ± 2.4	14.2 ± 0.1	+7.8 ± 0.6	5
M645C	*High K					2
L646A	−61.5 ± 2.6	21.8 ± 0.2	−60.0 ± 2.5	20.9 ± 0.2	+1.5 ± 0.9	5
I647A	−35.5 ± 3.2	18.1 ± 1.2	−19.1 ± 2.8	14.5 ± 0.7	+16.4 ± 2.4	5
G648A	*High K					2
S649A	−52.5 ± 2.4	19.8 ± 0.8	−35.4 ± 3.9	16.0 ± 0.4	+17.1 ± 1.9	3
L650A	−24.0 ± 5.2	19.1 ± 1.6	−13.7 ± 5.9	16.7 ± 1.5	+10.4 ± 1.5	3
M651A	−61.9, −58.6	17.2, 17.7	−44.9, −47.0	14.1, 16.1	+17.1, +11.6	2
Y652A	−38.5 ± 2.8	26.2 ± 2.7	−27.5 ± 3.7	21.2 ± 2.2	+11.0 ± 1.6	4
A653M	−27.4 ± 0.8	20.7 ± 0.0	−13.7 ± 0.4	15.5 ± 0.3	+13.7 ± 1.2	3
S654A	−45.6, −46.2	15.7, 16.4	−28.6, −26.3	13.4, 12.2	+17.0, +19.9	2
I655A	No expression					
F656T	−80.9 ± 4.4	23.2 ± 0.2	−49.8 ± 6.7	20.4 ± 0.8	+31.1 ± 2.3	3
G657A	−63.1 ± 1.9	24.3 ± 0.4	−43.0 ± 5.8	20.8 ± 1.0	+20.2 ± 4.0	3
N658A	Not measured, deactivation too rapid					
V659A	−21.1	17.6	−5.7	14.3	15.4	1
S660A	−40.5	19.2	−20.6	14.4	19.8	1
A661C	−48.8, −55.2	21.2, 21.2	−29.6, −31.2	15.1, 13.5	+19.2, +24.0	2
I662A	−69.6, −63.5	18.4, 22.0	−55.1, −48.9	17.1, 18.1	+14.4, +14.6	2
I663A	−60, −64.0	21.2, 16.0	−36.4, −49.8	16.8, 15.6	23.6, 14.1	2
Q664A	−48.0 ± 2.0	21.2 ± 0.2	−22.4 ± 2.2	17.6 ± 0.3	+25.6 ± 3.1	3
R665A	−65.2	21.7	−48.4	18.9	16.8	1
L666A	−41.0 ± 2.3	22.9 ± 2.4	−26.1 ± 2.0	16.3 ± 1.6	+14.9 ± 1.0	4
Y667A	−53.5	21.2	−34.8	16.7	18.8	1

*High K^+ extracellular solution

	% Increase in hERG1 tail currents at −140 mV	*N*
WT hERG1	36 ± 3.1	3
S641C	67 ± 14	3
M645C	148, 111	2
G648A	39, 48	2

Other Supporting Information

Dataset S1